Supporting Information for:

Large Hydrogen Bond Mismatch between TMAO and Urea Promotes Their Hydrophobic Association

Wen Jun Xie,[1,2,7] Seoncheol Cha,[1] Tatsuhiko Ohto,[3] Wataru Mizukami,[4] Yuezhi Mao,[5] Manfred Wagner,[1] Mischa Bonn,[1,*] Johannes Hunger,[1,*] and Yuki Nagata[1,6,*]

[1] Max Planck Institute for Polymer Research, Ackermannweg 10, D-55128, Mainz, Germany

[2] College of Chemistry and Molecular Engineering, Peking University, Beijing 100871, China

[3] Graduate School of Engineering Science, Osaka University, 1-3 Machikaneyama, Toyonaka, Osaka 560-8531, Japan

[4] Department of Energy and Material Sciences, Faculty of Engineering Sciences, Kyushu University, 6-1 Kasuga-Park, Fukuoka, Japan

[5] Kenneth S. Pitzer Center for Theoretical Chemistry, Department of Chemistry, University of California at Berkeley, Berkeley, CA 94720, USA

[6] Department of Theoretical and Computational Molecular Science, Institute for Molecular Science, Myodaiji, Okazaki, Aichi 444-8585, Japan

[7] Present address: Department of Chemistry, Massachusetts Institute of Technology, 77 Massachusetts Avenue, Cambridge, MA 02139,USA

*Correspondence: nagata@mpip-mainz.mpg.de, hunger@mpip-mainz.mpg.de, bonn@mpip-mainz.mpg.de

Table of contents

1. Computational Details

a. PMF calculation

We computed the potential of mean force (PMF) via the thermodynamic integration:[1]

$$W(r) = -\int_{r_0}^{r} \langle F(r') \rangle dr' + 2k_B T \ln\left(\frac{r}{r_0}\right) \quad \text{(S1)}$$

where $2k_B T \ln(r/r_0)$ represents the contribution of the volume-entropy, $F(r)$ is the force acting between the constrained C_{UREA} and O_{TMAO} atoms when the O_{TMAO}-C_{UREA} distance is equal to r, and r_0 represents the maximum O_{TMAO}-C_{UREA} separation for calculating the PMF.

b. *Ab initio* molecular dynamics simulation

In *ab initio* molecular dynamics (AIMD) simulations, all the molecules were deuterated. The Born-Oppenheimer AIMD simulations were performed with density functional theory. For the exchange and correlation functional, we used the Becke[2]/Lee-Yang-Parr [3](BLYP) together with the van der Waals correction of the Grimme's D3 method.[4] The van der Waals corrections are crucial to reproduce the correct water density and dynamics.[5-7] We employed the Goedecker-Teter-Hutter pseudopotentials[8] and the hybrid Gaussian and plane waves method. The TZV2P basis sets were used for the Gaussian wave functions. A 320 Ry cutoff was used for the auxiliary plane waves. Periodic boundary conditions were employed. The temperature was controlled by using the thermostats of canonical sampling through velocity rescaling[9] with a time constant of 300 fs. The timestep for integrating the equation of motion was set to 0.5 fs. The QUICKSTEP module implemented in the CP2K software package[10] was used in all the AIMD simulations.

c. Force field molecular dynamics simulation

We used the Kast model for TMAO,[11] the OPLS model for urea,[12] and SPC/E model for water[13] in force field molecular dynamics (FFMD) simulation. Such a combination of force field models has been used to show the strong direct hydrogen-bond (H-bond) between TMAO and urea.[14] Furthermore, we used two different TMAO models (the Shea model[15] and the Netz model[16]) and one urea model (the Kirkwood-Buff (KB) model[17]). The combination rules used for the LJ interactions in this study are as follows: $\sigma_{ij} =$

$\sqrt{\sigma_i \sigma_j}$ and $\epsilon_{\mathrm{ij}} = \sqrt{\epsilon_i \epsilon_j}$, where σ_i denotes the van der Waals (vdW) radius of atom *i*, and ϵ_i denotes the well depths of atom *i*. Such combination rules were also adopted in a recent study of association of hydrophobic molecules in TMAO-urea-water solution.[18]

For the analyses in Fig. 2a in the main text, we varied the charges of the O_{TMAO} and N_{TMAO} atoms in the Kast model.[11] The charges were obtained by combining the partial charges of the Kast model (q_{Kast})[11] and the Netz model (q_{Netz}).[16] In the Kast and the Netz TMAO models, the partial charges of the O_{TMAO} and N_{TMAO} atoms are different, while the partial charges of the C_{TMAO} and H_{TMAO} atoms are the same. We summarized the partial charges for TMAO models in Table S1.

For the analyses in Fig. S5, we varied the LJ radii of the C_{TMAO} and H_{TMAO} atoms in the Kast model. The radii were obtained by combining the LJ radii of the Kast TMAO model (σ_{Kast})[11] and the Netz TMAO model (σ_{Netz}).[16] In the Kast and Netz TMAO models, the LJ radii of the C_{TMAO} and H_{TMAO} atoms are different, while the O_{TMAO} and N_{TMAO} atoms have the same LJ radii. The well depths of the LJ potentials are the same for all the atoms in the two models. We summarized the LJ radii for TMAO models in Table S2.

For the analyses in Fig. 2b in the main text, we varied charges of urea by scaling the partial charges of the OPLS urea model[12] with different factors. We summarized the partial charges in the urea models in Table S3.

For all these simulations, temperature was controlled by using the thermostats of canonical sampling through velocity rescaling[9] with a time constant of 300 fs. The timestep for integrating the equation of motion was set to 0.5 fs. The CP2K software package[10] was used in all the FFMD simulations.

Table S1. The partial charges for TMAO models used for Fig. 2a in the main text

Combination of charges	O_{TMAO} charge (*e*)	N_{TMAO} charge (*e*)
q_{Kast}[11]	-0.650	0.440
$0.75q_{Kast} + 0.25q_{Netz}$	-0.715	0.505
$0.50q_{Kast} + 0.50q_{Netz}$	-0.780	0.570
$0.25q_{Kast} + 0.75q_{Netz}$	-0.845	0.635
q_{Netz}[16]	-0.910	0.700

Table S2. The LJ radii for TMAO models used for Fig. S5

Combination of vdW radii	vdW radius of C_{TMAO} (Å)	vdW radius of H_{TMAO} (Å)
σ_{Kast}11	3.041	1.775
$0.75\sigma_{Kast} + 0.25\sigma_{Netz}$	3.18075	1.8565
$0.50\sigma_{Kast} + 0.50\sigma_{Netz}$	3.3205	1.938
$0.25\sigma_{Kast} + 0.75\sigma_{Netz}$	3.46025	2.0195
σ_{Netz}16	3.600	2.101

Table S3. The partial charges for urea models used for Fig. 2b in the main text

Scaling OPLS Charge	C_{UREA} charge (*e*)	O_{UREA} charge (*e*)	N_{UREA} charge (*e*)	H_{UREA} charge (*e*)
$0.50q_{OPLS}$	0.0710	-0.195	-0.271	0.1665
$0.75q_{OPLS}$	0.1065	-0.2925	-0.4065	0.24975
q_{OPLS}[12]	0.142	-0.390	-0.542	0.333

d. TMAO-urea-water system

We performed AIMD and FFMD simulations of the TMAO-urea-water mixture for computing the TMAO-urea PMF. For AIMD simulations, the simulation cell of TMAO-urea-water mixture with its size of (17.075 Å)^3 contained one deuterated TMAO (d-

TMAO) molecule, one deuterated urea (d-urea) molecule and 159 D_2O molecules, resulting in a density of 1.112 g/cm^3. This corresponds to 1.001 g/cm^3 for the system with all hydrogen atoms. The system temperature was set to 380 K (for details on the effect of temperature see section 2 below). For computing the PMF, we constrained the distance between O_{TMAO} and C_{UREA} ranging from 3.60 to 6.60 Å with an interval of 0.25 Å. The constraint was made by using the SHAKE algorithm.[19] The time series of the constraint forces were used for computing the PMF profile using equation (S1). With this constraint, we ran the NVT simulations.

For the FFMD simulation, we performed 8 ns FFMD runs after 1 ns equilibration in the canonical ensemble. We computed the average force for every 1 ns simulation data at each TMAO-urea separation.

For the AIMD simulation, the initial configuration at a separation of 5.10 Å between TMAO and urea was obtained from the equilibrated FFMD simulation. After 2 ps AIMD simulation for equilibration, we repeated the gradual elongation/shortening of the intermolecular distances and the equilibration with AIMD. We performed 8 independent AIMD simulations. For each constrained separation simulation, we obtained a 20 ps long trajectory for analysis after 2 ps NVT runs to equilibrate the system. In total we obtained 2.08 ns AIMD trajectories.

e. TMAO-water system

For computing the dynamics of TMAO-water H-bonds, we performed an AIMD simulation of a d-TMAO-D_2O system and a FFMD simulation of a TMAO-H_2O system. The system contained one TMAO (d-TMAO) and 100 H_2O (D_2O) molecules for the FFMD (AIMD) simulation. The size of the simulation box was set to (14.62 Å)^3. The target temperature in the NVT ensemble was set to 320 K.

For the FFMD simulation, we used the SPC/E model for water. We used the Kast TMAO model as well as the modified TMAO models (see Table S1). After 1 ns equilibration, we obtained 500 ps FFMD simulation data for analysis. The 643 ps AIMD trajectory was taken from Ref. 20.

f. Urea-water system

For computing the dynamics of urea-water H-bonds, we performed an AIMD simulation for a d-urea-D_2O system and a FFMD simulation for a urea-H_2O system. The system contained one urea (d-urea) and 100 H_2O (D_2O) molecules for the FFMD (AIMD) simulation. The size of the simulation box was set to $(14.60\ \text{Å})^3$. The target temperature in the NVT ensemble was set to 320 K.

For the FFMD simulation, we used the SPC/E model for water. The data in Fig. 3b in the main text were obtained using the OPLS urea model and the urea models listed in Table S3. After 1 ns equilibration, we obtained 500 ps FFMD trajectory for analysis. For the AIMD simulation, two different sets of initial coordinates were obtained from the FFMD simulations with the OPLS urea model + SPC/E water model. By using these initial coordinates, we performed 10 ps NVT runs to equilibrate the systems. Subsequently, we carried out over 80 ps AIMD runs. We finally obtained a total of 165 ps AIMD trajectories, which were used for computing the H-bond dynamics.

g. Neat water system

For computing the dynamics of water-water H-bonds, we performed AIMD simulations for D_2O and FFMD simulation for H_2O. For both simulations, the system contained 64 water molecules and the size of the simulation box was set to $(12.429\ \text{Å})^3$. The target temperature in the NVT ensemble was set to 320 K.

For the FFMD simulation, the SPC/E model for water was used. After 1 ns equilibration, we obtained 500 ps FFMD trajectory for analysis. The 475 ps AIMD trajectory was taken from Ref. 20.

h. NMR chemical shift calculation

We computed ^{1}H NMR chemical shifts of TMAO for the aqueous TMAO and TMAO-urea solution by using *ab initio* calculations. For this computation, took a TMAO molecule and water molecules surrounding the TMAO molecule from the AIMD trajectories. The water molecules were included in the chemical shift calculations, when any atoms of water is within 3 Å from any atom of TMAO. We used 100 AIMD snapshots of TMAO in water and TMAO-urea in water with the fixed distances of r = 3.85 and 5.60 Å. By averaging the computed chemical shifts over these 100 snapshots, we obtained the

values of the chemical shifts for TMAO in water, TMAO with the O_{TMAO}…H_{UREA} H-bond (r = 3.85 Å), and TMAO with the hydrophobic association with urea (r = 5.60 Å).

NMR magnetic shielding tensors were computed at B3LYP, PBE0, and mPW1LYP/def2-TZVPP level of theory using gauge independent atomic orbitals (GIAO). Furthermore, to examine whether the water molecules beyond the 3.0 Å spheres around TMAO affects the NMR shift, we considered a larger system, which included the water molecules within 5.0 Å from TMAO. This calculation was done with the ONIOM technique[21], where the lower-level NMR calculations for the large system was done at the B3LYP/6-31G** level of theory.

The NMR chemical shift δ is given by the difference in magnetic shielding constants from a reference σ_{ref}:

$$\delta = (\sigma_{\mathrm{ref}} - \sigma)/f \qquad \text{(S2)}$$

where f denotes a scaling factor. In this study, we set f and σ_{ref} to 1.1 and 31.713 ppm, respectively. σ_{ref} of 31.713 ppm was obtained from the computed ^{1}H magnetic shielding constant of TMS at B3LYP/def2-TZVPP. For all the NMR calculations, we used the polarizable continuum model to account for water beyond the explicitly treated solvation shells. We employed Gaussian 16 program suits revision A.[22]

Our ^{1}H chemical shift calculations for TMAO in both explicit water and implicit solvent model show that the chemical shifts of nine H atoms of TMAO are not similar. Since TMAO has a C_{3v} point group symmetry, the nine H atoms can be classified into two categories; one consists of the six H atoms closer to the O_{TMAO} atom (pointed by arrows in Fig. S1(a)), while the other consists of the rest of three H atoms. These sub-ensembles of the H atoms provide largely different chemical shifts (The differences are 0.33 ppm in the implicit solvent model calculation and 0.35 ± 0.04 ppm in the explicit water calculation). For the chemical shifts calculation of TMAO in water and TMAO-urea in water with r = 3.85 Å, we calculated the shifts by averaging individual chemical shifts over these six H atoms.

For the chemical shift of TMAO-urea in water with r = 5.60 Å, we focused on the two H atoms that are close to urea. Gas-phase *ab initio* calculation of a hydrophobically associates TMAO-urea system with suggested that urea affects the NMR chemical shifts of one or at most two H atoms of TMAO and the influence of urea on the other H atoms of TMAO is quite limited. Thus, we selected two H atoms among the six H atoms near the O_{TMAO} atom and averaged the chemical shifts for these two H atoms. For choosing these two H atoms next to urea, we used the criteria of the intermolecular distance of

C_{UREA}…H_{TMAO} being less than 4.8 Å and the angle of C_{UREA}…H_{TMAO}-C_{TMAO} being larger than 90^0. A typical conformation of the TMAO-urea with r = 5.6 Å are depicted in Fig. S1(b), together with the chosen two H atoms neighboured to urea (point by the arrows).

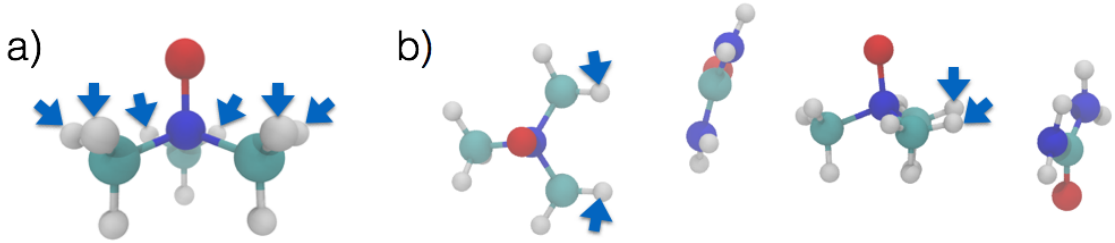

Figure S1. (a) Schematics of TMAO molecule. The arrows point the six H atoms which are close to the O_{TMAO} atom. (b) Schematics of TMAO-urea conformation at r = 5.60 Å. The arrows point at the two H atoms near urea amongst these six H atoms.

2. Supporting Data

a. Effect of temperature on the TMAO-urea PMF

In the MD simulations for calculating the PMF, we used relatively high temperature (380 K) to accelerate the sampling in the whole phase-space. To examine the effects of the elevated temperature on the PMF, we also carried out the FFMD simulation at 340 K and 300 K and compared the PMF at 380 K with those at 340 K and 300 K. The simulation conditions such as cell size and ensemble were the same as the FFMD simulation at 380 K.

Fig. S2 displays the PMFs at different temperatures. The two minima are commonly found at these temperatures. Furthermore, the difference in the PMFs at 300 K and 380 K is 0.12 kcal/mol at maximum, which is much smaller than the PMF difference between the FFMD and AIMD simulation (see Fig. 1 in the main text). Thus, the elevated temperature at 380 K does not significantly affect the trends in the reported PMFs.

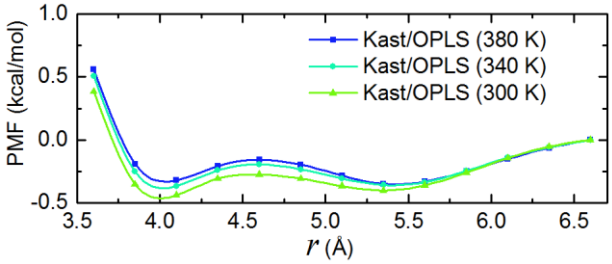

Figure S2. Effect of temperature on the TMAO-urea PMF.

b. Effect of simulation cell size on the TMAO-urea PMF

To examine the effect of the simulation cell size on the PMF, we calculated the PMF using the large simulation cell in FFMD simulation. This simulation cell contained one TMAO molecule, one urea molecule and 610 water molecules with a cell size of $(26.40\ \text{Å})^3$, resulting in a density of 1.00 g/cm^3. The separation distance r ranges from 3.60 Å to 10.60 Å with an interval of 0.25 Å. The other simulation conditions such as target temperature and ensemble s were the same as the FFMD simulation with a simulation cell size of $(17.075\ \text{Å})^3$.

The comparison between the constraint force and PMF in the large simulation cell ($(26.40\ \text{Å})^3$) and the small simulation cell ($(17.075\ \text{Å})^3$) are shown in Fig. S3. The values of intermolecular constraint force for $r < 6.60$ Å coincide quite well between FFMD simulations with the large simulation cells and with the small simulation cells. This demonstrates that the cell size of $(17.075\ \text{Å})^3$ suffices to compute the PMF of TMAO and urea.

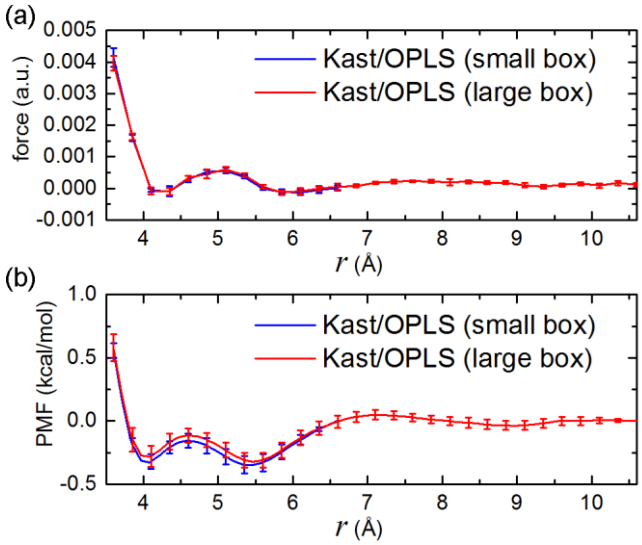

Figure S3. Comparison of constraint force and PMF in the FFMD simulation with different simulation cell sizes. (a) Constraint force. (b) PMF. The simulation boxes with cell sizes of $(26.40\ \text{Å})^3$ and $(17.075\ \text{Å})^3$ are respectively denoted as large box and small box in the figure legend.

c. PMF obtained from long AIMD simulation trajectories

In the main text, we reported the TMAO-urea PMF by averaging the values over 8 independent AIMD trajectories (Fig. 1). Due to the high computational cost of AIMD simulation, the simulation length for each TMAO-urea separation in each independent trajectory was 20 ps. To further confirm that the AIMD PMF data is fully converged, we compare the AIMD PMF data for 8 × 20 ps samples with that obtained from a 130 ps AIMD trajectory.

The PMF computed from the 130 ps AIMD trajectories is shown in Fig. S4 (denoted as "long-time"). The PMF have a shallow minimum in $5.3\ \text{Å} \leq r \leq 5.7\ \text{Å}$ and is increasingly unfavorable with a short $O_{TMAO}\ldots C_{UREA}$ separation of $r < 5.3$ Å. These trends are consistent with the PMF reported in the main text.

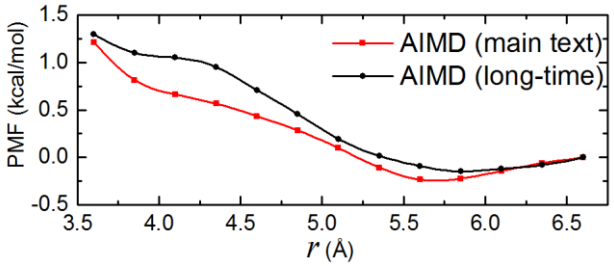

Figure S4. Comparisons of PMFs in different AIMD simulation trajectories. The PMF obtained from eight independent trajectories (8 × 20 ps) is shown in red, while the PMF using the long-time AIMD 130 ps trajectory for a single initial coordinate is shown in black.

d. Hydrophobic interaction between TMAO and urea

The variation of LJ radius should affect the hydrophobic interactions of TMAO. To measure how the PMFs are affected by this LJ radius, we varied the radius parameter of the LJ potential for the H_{TMAO} and C_{TMAO} atoms. The PMFs simulated with various LJ radii are shown in Fig. S5. The larger LJ radius of the TMAO methyl groups shifts the location of the PMF minimum at r = 5.4 Å to longer r. This indicates that the PMF minimum at r = 5.4 Å likely originates from hydrophobic interaction between TMAO and urea. Contrarily, the variation of the LJ radius of the methyl group does not change the relative depths of the PMF minima at r = 4.1 Å and r = ~5.4 Å, suggesting that the PMF minima at r = 4.1 Å are not due to hydrophobic interaction.

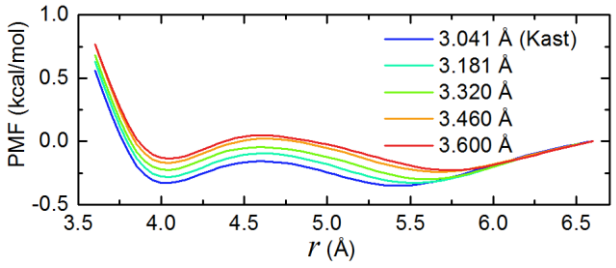

Figure S5. PMFs of the FFMD simulation when varying the LJ radius of C_{TMAO} and H_{TMAO} atoms.

e. H-bond number between TMAO and urea

TMAO and urea can form H-bond in which TMAO acts as H-bond acceptor and urea is H-bond donor. As mentioned in the main text, the H-bond number is defined as unity when 1.59 Å < $r_{O\cdots H}$ < 2.27 Å,[23] where O and H denote the oxygen and hydrogen atoms involved in the H-bond formation, respectively. The average H-bond number between TMAO and urea in AIMD simulation was shown in Fig. S6. We found directly H-bonded TMAO-urea conformation at $r \leq$ ~4.1 Å, which is consistent with the assignment made in the main text.

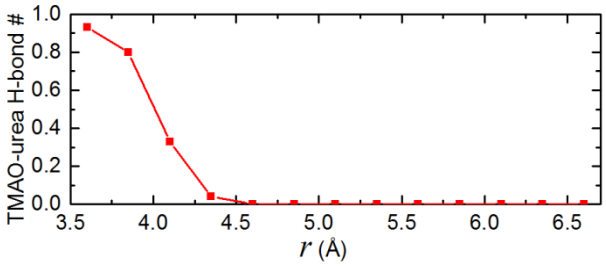

Figure S6. Average H-bond number between TMAO and urea in AIMD simulation.

f. H-bond dynamics

The H-bond dynamics were computed as the H-bond time correlation function;[24]

$$P_{\mathrm{HB}}(t) = \frac{\langle h(0)h(t)\rangle}{\langle h(0)\rangle} \qquad \text{(S3)}$$

where $h(t)$ is unity when the H-bond is formed, 0 otherwise. The same H-bond definition as the above calculation was used for evaluating the H-bond dynamics.

Fig. 3 in the main text shows the more pronounced difference in the $O_{TMAO}\cdots H_W$ and $H_{UREA}\cdots O_W$ H-bond dynamics in the AIMD simulation as compared to the FFMD simulation. Here, we plotted the variation of the H-bond dynamics when we changed the charges of TMAO (See Table S1) and of urea (See Table S3). We can see that the increase in the absolute value of the O_{TMAO} charge slows down the H-bond dynamics of TMAO-water, and a decrease in the H_{UREA} charge accelerates the H-bond dynamics of urea-water (Fig. S7).

Further data are obtained by using the KB urea model.[17] Fig. S8 depicts the comparison of the H-bond dynamics of the OPLS urea model and the KB urea model.

The H-bond dynamics of the KB urea is faster than the OPLS urea. This result that the KB urea model shows faster H-bond dynamics than the OPLS urea model is consistent with KB model having weaker H-bond with water. [17]

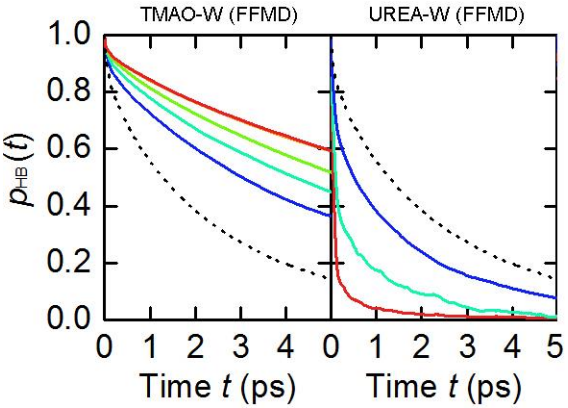

Figure S7. (a) O_{TMAO}…H_W H-bond dynamics and (b) H_{UREA}…O_W H-bond dynamics simulated in the FFMD. The color codes of the solid lines are the same as Fig. 2(a) and (b), respectively, while the dotted black line represents the O_W…H_W H-bond dynamics.

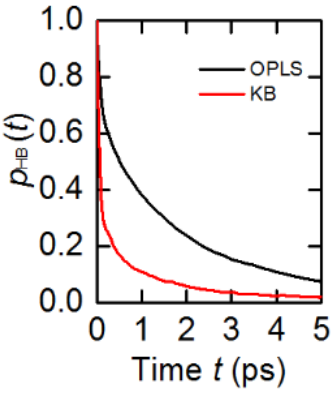

Figure S8. Comparison of H-bond dynamics of the OPLS urea model and the KB urea model.

g. PMFs using the Netz TMAO model, the Shea TMAO model, and the KB urea model

It has been shown that both the Kast TMAO model and OPLS urea models are not perfect; the poor reproduction of the macroscopic observables such as the concentration-dependent density of aqueous TMAO solutions and the solution activity coefficients with

the Kast TMAO model was pointed out in previous studies[15, 16], motivating improvement of the force field models. New force field models including the Shea[15] and Netz[16] TMAO models were developed recently, in addition to several other models.[25, 26] The Shea TMAO model could reproduce the number of hydration water and the Netz TMAO model could reproduce the H-bond dynamics of water.[27] The KB urea model can reproduce solution thermodynamics of urea-water system and improves the performance of urea self-aggregation.[17] The combinations of the KB urea and the Kast, Netz, Shea for TMAO were also used to study the solvation of amino acids.[28]

Based on these findings, we also calculated the TMAO-urea PMF using recently developed force field models (the Shea TMAO model[15] and the Netz TMAO model,[16] together with the KB urea model[17]). The PMFs using the OPLS urea model and the KB urea model are shown in Fig. S9(a) and (b), respectively. At r = ~4.1 Å, the values of the PMFs follow the order of Netz model > Shea model > Kast model, independent of the urea model. The speed of the H-bond dynamics also follows the order of Netz model < Shea model < Kast model (Fig.4 in Ref. 27). Consistent with our conclusion in the main text, we can correlate the order of the H-bond dynamics with the PMF. The Netz TMAO model shows the slowest H-bond dynamics, which has the largest deviation with urea H-bond dynamics. Therefore, the PMF at r = ~4.1 Å using the Netz TMAO model is the highest.

When we used the KB urea model instead of the OPLS model, the PMFs increase at r = ~4.1 Å. We have seen that the KB urea model shows a faster H-bond dynamics than the OPLS urea (Fig. S8). The deviation between the H-bond dynamics of TMAO and urea would increase when using the KB urea. Thus, the PMF using the KB urea is higher than that using the OPLS urea.

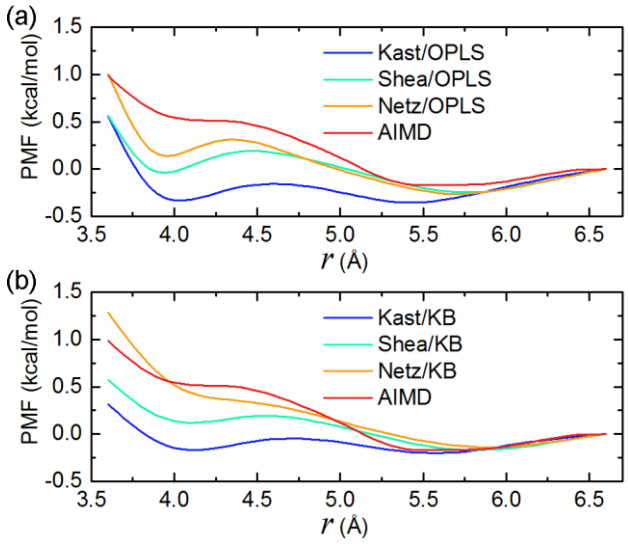

Figure S9. TMAO-urea PMFs using different TMAO models and urea models. The PMF obtained from AIMD simulation is also shown for comparison.

h. NMR chemical shift calculation

The computed chemical shifts at the ONIOM theory are summarized in Table S4. The average NMR ^{1}H chemical shifts of TMAO increases upon H-bond formation between urea and TMAO (r = 3.85 Å), while it decreases when urea associates hydrophobically to TMAO (r = 5.60 Å). These trends can be seen for B3LYP, PBE0, and mPW1LYP functionals. Furthermore, we obtained the same trend, even when we did not use the ONIOM calculation.

As will be explained in Sec. 3d in this Supporting Information, the experimental NMR data shows the up-field shifts for ^{1}H upon the addition of urea into the aqueous TMAO solution. This is consistent with the scenario that TMAO and urea is hydrophobically associated, whereas this is at odds with the scenario that TMAO and urea can form the direct H-bonds. Thus, the experimentally measured up-field shift indicates that TMAO-urea interactions are governed by the hydrophobic interaction.

Table S4. Computed NMR proton chemical shifts of TMAO using the ONIOM-NMR technique. The unit of chemical shifts is ppm. Parenthesis values indicate standard errors.

	B3LYP	PBE0	mPW1LYP
TMAO w/o urea	3.58 (0.03)	3.69 (0.03)	3.55 (0.03)
TMAO w/ urea at r =3.85 Å	3.80 (0.03)	3.91 (0.04)	3.77 (0.03)
TMAO near urea at r = 5.60 Å	3.45 (0.04)	3.57 (0.04)	3.42 (0.04)

3. Experimental Details

a. Polarization-resolved femtosecond infrared pump-probe experiments

Femtosecond laser pulses from a regenerative amplifier (Spectra Physics, Spitfire Ace, 800 nm, 35 fs, 1 kHz repetition rate) were converted into mid-IR pulses (ω = 2500 cm^{-1} peak frequency and ~ 400 cm^{-1} FWHM) using an optical parametric amplifier together with a difference frequency generation stage (Light conversion, TOPAS) and split into pump and probe pulses. A half-wave plate was used to rotate the pump polarization to 45º with respect to the probe polarization. The timing of the pump pulses was delayed relative to the probe pulse using a translational stage and both the pump and the probe pulses are focused into the sample and re-collimated using off-axis parabolic mirrors. For the probe pulse, the component parallel and perpendicular to the pump polarization can be selected by using a polarizer, giving the parallel ($\Delta a_{\parallel}(\omega, t)$) and perpendicular ($\Delta a_{\perp}(\omega, t)$) transient (pump-induced) absorption spectra, respectively. Both components were spectrally dispersed onto a 2 × 32 MCT (mercury-cadmium-telluride) array, where both the intensity with and without the pump is detected (I_{probe}). For active noise reduction a reference beam was detected simultaneously and the pump beam was modulated at 500Hz using an optical chopper.

The transient absorption of the samples is given by

$$\Delta a = -\ln[I_{probe,with\ pump}/I_{probe,without\ pump}]. \quad \text{(S4)}$$

Isotropic transient absorption, which does not contain rotational contributions, but represents only energy relaxation and dissipation

$$\Delta a_{iso}(\omega, t) = \frac{\Delta a_{\parallel}(\omega,t)+2\Delta a_{\perp}(\omega,t)}{3} \quad \text{(S5)}$$

was constructed and fitted by a two-step relaxation model to extract the contributions of vibrational excitation and the heating to the signal.[29] The anisotropy of the excitation, as shown in the main manuscript, $R(\omega,t)$ was calculated by

$$R(\omega,t) = \frac{\Delta a_{\parallel}{}'(\omega,t) - \Delta a_{\perp}{}'(\omega,t)}{\Delta a_{\parallel}{}'(\omega,t) + 2\Delta a_{\perp}{}'(\omega,t)}, \quad \text{(S6)}$$

where $\Delta a_{\parallel}{}'(\omega,t)$ and $\Delta a_{\perp}{}'(\omega,t)$ correspond to the parallel and perpendicular transient spectra, corrected for the heating contributions (for details see refs 30, 31).

b. Samples

Trimethylamine-N-oxide dihydrate (SigmaAldrich, >99%) and urea (SigmaAlrich >99%) were used without further purification. All samples were prepared by weighing the appropriate amount of trimethylamine-N-oxide dihydrate and urea into volumetric flask and mixing them with 5wt% heavy water (Sigma-Aldrich, 99.9 %D) in Milli-Q water (Millipore , 18.2 MΩ cm at 25 deg).

c. Isotropic relaxation

As indicated in the main text of the manuscript, both HOD molecules H-bonded to water and H-bonded to TMAO contribute to the observed transient signals. Both TMAO and urea do not affect the isotropic decay at the center of the $O_W\ldots D_W\text{-}O_W$ H-bonded O-D stretching peak at 2500 cm^{-1} (see Fig. S10(b)). As some of us have shown previously,[20, 27] the $O_{TMAO}\ldots D_W\text{-}O_W$ are centered at red-shifted frequencies, relative to $O_W\ldots D_W\text{-}O_W$ H-bonded O-D groups. Consistent with this earlier study, at a TMAO concentration as low as 2 M the isotropic dynamics at 2470 cm^{-1} is hardly affected by the presence of these red-shifted $O_{TMAO}\ldots D_W\text{-}O_W$ groups (see Fig. S10(a)). Noteworthy, urea virtually not affects the isotropic decays at both frequencies, which indicates that urea does not alter the H-bonded structure of the studied solutions significantly.

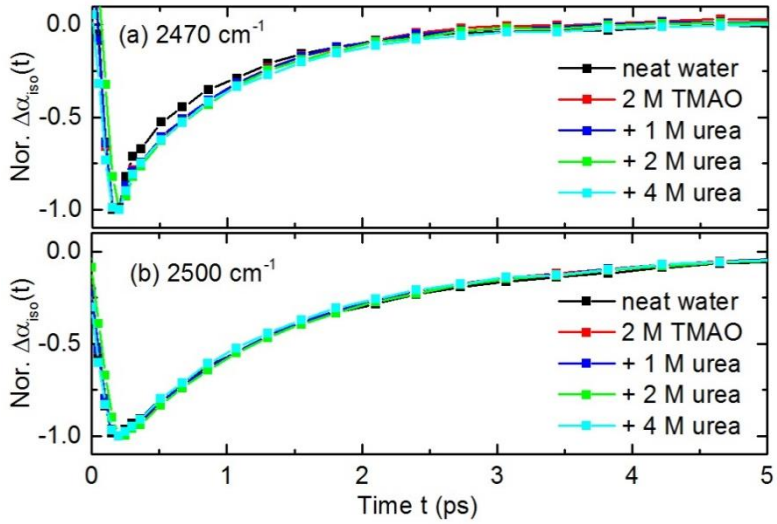

Figure S10. Normalized time-dependent transient absorption, $\Delta\alpha_{iso}(t)$ at (a) 2470 cm^{-1} and (b) 2500 cm^{-1} for aqueous solutions (5 wt% HOD in H_2O) containing different concentrations of TMAO and urea.

d. ^{1}H NMR measurement

To determine the chemical environment of the hydrophobic CH_3 groups of TMAO as a function of urea concentration we performed ^{1}H-NMR experiments. ^{1}H-NMR spectra of the solutions in H_2O were recorded using a 850 MHz Bruker AVANCE III system equipped with a 5 mm triple resonance TXI ^{1}H/^{13}C/^{15}N probe with a *z*-gradient. For the proton NMR spectra 16 to 64 transients (depending on the urea concentration) using a 9 μs long 90° pulse and a 17000 Hz spectral width together with a recycling delay of 10 s. For referencing, a sealed capillary with DMSO-d_6 was placed inside the 5 mm tube with a small fraction of DMSO-d_5H. The temperature was controlled to 298.3 K with a VTU (variable temperature unit) and an accuracy of +/- 0.1 K.

Experiments were performed using a constant concentration of TMAO (0.35 mol/L) with increasing concentration of C13-urea (0-0.49 mol/L). As can be seen in Figs. 5 and S11, the NMR chemical shifts of TMAO's CH_3 groups experience a very minor, gradual up-field shift with increasing concentration of urea. Together with the shift computation (see Sec. 2.h. in this SI), the experimentally observed up-field shift provides evidence for the proximity of urea to TMAO's hydrophobic CH_3 groups.

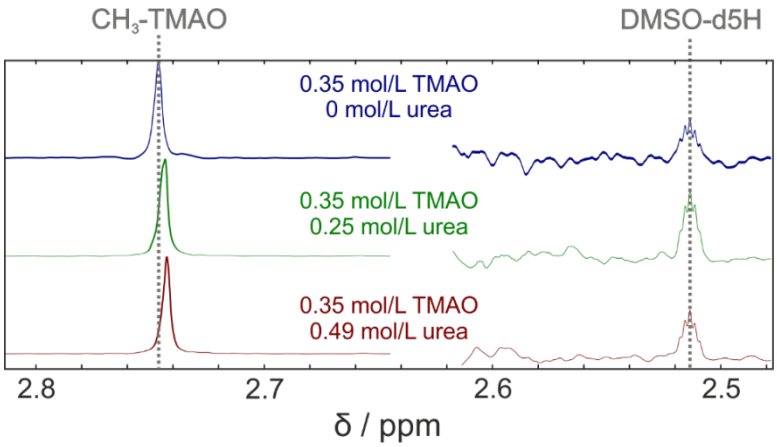

Figure S11: (left) Representative ^{1}H NMR spectra for solutions with a constant concentration of TMAO and varying concentration of C13-urea. The signal at ~2.73 ppm due to the CH_3 groups of TMAO shifts up-field with increasing urea concentration, while the signal due to residual DMSO-d5H at ~2.51 ppm, which was used as reference, remains unchanged

References

1. Trzesniak, D., Kunz, A. P. E., and van Gunsteren, W. F. (2007). A comparison of methods to compute the potential of mean force. ChemPhysChem 8, 162-169.
2. Becke, A. D. (1988). Density-functional exchange-energy approximation with correct asymptotic-behavior. Phys. Rev. A 38, 3098-3100.
3. Lee, C. T., Yang, W. T., and Parr, R. G. (1988). Development of the colle-salvetti correlation-energy formula into a functional of the electron-density. Phys. Rev. B 37, 785-789.
4. Grimme, S., Antony, J., Ehrlich, S., and Krieg, H. (2010). A consistent and accurate ab initio parametrization of density functional dispersion correction (DFT-D) for the 94 elements H-Pu. J. Chem. Phys. 132, 154104.
5. Lin, I. C., Seitsonen, A. P., Tavernelli, I., and Rothlisberger, U. (2012). Structure and dynamics of liquid water from ab initio molecular dynamics-comparison of BLYP, PBE, and REVPBE density functionals with and without van der waals corrections. J. Chem. Theory Comput. 8, 3902-3910.
6. Lin, I. C., Seitsonen, A. P., Coutinho-Neto, M. D., Tavernelli, I., and Rothlisberger, U. (2009). Importance of Van der Waals interactions in liquid water. J. Phys. Chem. B 113, 1127-1131.

7. Kuhne, T. D., Pascal, T. A., Kaxiras, E., and Jung, Y. (2011). New insights into the structure of the vapor/water interface from large-scale first-principles simulations. J. Phys. Chem. Lett. 2, 105-113.
8. Goedecker, S., Teter, M., and Hutter, J. (1996). Separable dual-space gaussian pseudopotentials. Phys. Rev. B 54, 1703-1710.
9. Bussi, G., Donadio, D., and Parrinello, M. (2007). Canonical sampling through velocity rescaling. J. Chem. Phys. 126, 014101.
10. http://www.cp2k.org/
11. Kast, K. M., Brickmann, J., Kast, S. M., and Berry, R. S. (2003). Binary phases of aliphatic N-oxides and water: Force field development and molecular dynamics simulation. J. Phys. Chem. A 107, 5342-5351.
12. Duffy, E. M., Kowalczyk, P. J., and Jorgensen, W. L. (1993). Do denaturants interact with aromatic-hydrocarbons in water. J. Am. Chem. Soc. 115, 9271-9275.
13. Berendsen, H. J. C., Grigera, J. R., and Straatsma, T. P. (1987). The missing term in effective pair potentials. J. Phys. Chem. 91, 6269-6271.
14. Paul, S., and Patey, G. N. (2007). Structure and interaction in aqueous urea-trimethylamine-N-oxide solutions. J. Am. Chem. Soc. 129, 4476-4482.
15. Larini, L., and Shea, J. E. (2013). Double resolution model for studying tmao/water effective interactions. J. Phys. Chem. B 117, 13268-13277.
16. Schneck, E., Horinek, D., and Netz, R. R. (2013). Insight into the molecular mechanisms of protein stabilizing osmolytes from global force-field variations. J. Phys. Chem. B 117, 8310-8321.
17. Weerasinghe, S., and Smith, P. E. (2003). A Kirkwood-Buff derived force field for mixtures of urea and water. J. Phys. Chem. B 107, 3891-3898.
18. Ganguly, P., van der Vegt, N. F., and Shea, J. E. (2016). Hydrophobic association in mixed urea-TMAO solutions. J. Phys. Chem. Lett. 7, 3052-3059.
19. Ryckaert, J.-P., Ciccotti, G., and Berendsen, H. J. C. (1977). Numerical integration of the cartesian equations of motion of a system with constraints: Molecular dynamics of n-alkanes. J. Comput. Phys. 23, 327-341.
20. Usui, K., Hunger, J., Sulpizi, M., Ohto, T., Bonn, M., and Nagata, Y. (2015). Ab initio liquid water dynamics in aqueous tmao solution. J. Phys. Chem. B 119, 10597-10606.
21. Karadakov, P. B., and Morokuma, K. (2000). ONIOM as an efficient tool for calculating NMR chemical shielding constants in large molecules. Chem. Phys. Lett. 317, 589-596.

22. Gaussian 16, R. A., Frisch, M. J.; Trucks, G. W.; Schlegel, H. B.; Scuseria, G. E.; Robb, M. A.; Cheeseman, J. R.; Scalmani, G.; Barone, V.; Petersson, G. A.; Nakatsuji, H.; Li, X.; Caricato, M.; Marenich, A. V.; Bloino, J.; Janesko, B. G.; Gomperts, R.; Mennucci, B.; Hratchian, H. P.; Ortiz, J. V.; Izmaylov, A. F.; Sonnenberg, J. L.; Williams-Young, D.; Ding, F.; Lipparini, F.; Egidi, F.; Goings, J.; Peng, B.; Petrone, A.; Henderson, T.; Ranasinghe, D.; Zakrzewski, V. G.; Gao, J.; Rega, N.; Zheng, G.; Liang, W.; Hada, M.; Ehara, M.; Toyota, K.; Fukuda, R.; Hasegawa, J.; Ishida, M.; Nakajima, T.; Honda, Y.; Kitao, O.; Nakai, H.; Vreven, T.; Throssell, K.; Montgomery, J. A., Jr.; Peralta, J. E.; Ogliaro, F.; Bearpark, M. J.; Heyd, J. J.; Brothers, E. N.; Kudin, K. N.; Staroverov, V. N.; Keith, T. A.; Kobayashi, R.; Normand, J.; Raghavachari, K.; Rendell, A. P.; Burant, J. C.; Iyengar, S. S.; Tomasi, J.; Cossi, M.; Millam, J. M.; Klene, M.; Adamo, C.; Cammi, R.; Ochterski, J. W.; Martin, R. L.; Morokuma, K.; Farkas, O.; Foresman, J. B.; Fox, D. J. Gaussian, Inc., Wallingford CT, 2016.
23. Kuo, I. F. W., and Mundy, C. J. (2004). An ab initio molecular dynamics study of the aqueous liquid-vapor interface. Science 303, 658-660.
24. Luzar, A., and Chandler, D. (1996). Hydrogen-bond kinetics in liquid water. Nature 379, 55-57.
25. Holzl, C., Kibies, P., Imoto, S., Frach, R., Suladze, S., Winter, R., Marx, D., Horinek, D., and Kast, S. M. (2016). Design principles for high-pressure force fields: Aqueous TMAO solutions from ambient to kilobar pressures. J. Chem. Phys. 144, 144104.
26. Canchi, D. R., Jayasimha, P., Rau, D. C., Makhatadze, G. I., and Garcia, A. E. (2012). Molecular mechanism for the preferential exclusion of TMAO from protein surfaces. J. Phys. Chem. B 116, 12095-12104.
27. Usui, K., Nagata, Y., Hunger, J., Bonn, M., and Sulpizi, M. (2016). A new force field including charge directionality for TMAO in aqueous solution. J. Chem. Phys. 145, 064103.
28. Ganguly, P., Hajari, T., Shea, J. E., and van der Vegt, N. F. A. (2015). Mutual exclusion of urea and trimethylamine N-oxide from amino acids in mixed solvent environment. J. Phys. Chem. Lett. 6, 581-585.
29. Rezus, Y. L., and Bakker, H. J. (2006). Orientational dynamics of isotopically diluted H2O and D2O. J. Chem. Phys. 125, 144512.
30. Rezus, Y. L. A., and Bakker, H. J. (2006). Effect of urea on the structural dynamics of water. Proc. Natl. Acad. Sci. USA 103, 18417-18420.

31. Rezus, Y. L. A., and Bakker, H. J. (2007). Observation of immobilized water molecules around hydrophobic groups. Phys. Rev. Lett. 99, 148301.